The Astrophysical Journal, 691:596–610, 2009 January 20 doi:10.1088/0004-637X/691/1/596

HABITABLE CLIMATES: THE INFLUENCE OF OBLIQUITY

David S. Spiegel[1,2], Kristen Menou[1], and Caleb A. Scharf[1,3]
[1] Department of Astronomy, Columbia University, 550 West 120th Street, New York, NY 10027, USA; dave@astro.columbia.edu, kristen@astro.columbia.edu, caleb@astro.columbia.edu
[2] Department of Astrophysical Sciences, Princeton University, Peyton Hall, Princeton, NJ 08544, USA
[3] Columbia Astrobiology Center, Columbia University, 550 West 120th Street, New York, NY 10027, USA
Received 2008 July 25; accepted 2008 September 9; published 2009 January 16

ABSTRACT

Extrasolar terrestrial planets with the potential to host life might have large obliquities or be subject to strong obliquity variations. We revisit the habitability of oblique planets with an energy balance climate model (EBM) allowing for dynamical transitions to ice-covered snowball states as a result of ice-albedo feedback. Despite the great simplicity of our EBM, it captures reasonably well the seasonal cycle of global energetic fluxes at Earth's surface. It also performs satisfactorily against a full-physics climate model of a highly oblique Earth-like planet, in an unusual regime of circulation dominated by heat transport from the poles to the equator. Climates on oblique terrestrial planets can violate global radiative balance through much of their seasonal cycle, which limits the usefulness of simple radiative equilibrium arguments. High obliquity planets have severe climates, with large amplitude seasonal variations, but they are not necessarily more prone to global snowball transitions than low obliquity planets. We find that terrestrial planets with massive CO_2 atmospheres, typically expected in the outer regions of habitable zones, can also be subject to such dynamical snowball transitions. Some of the snowball climates investigated for CO_2-rich atmospheres experience partial atmospheric collapse. Since long-term CO_2 atmospheric build-up acts as a climatic thermostat for habitable planets, partial CO_2 collapse could limit the habitability of such planets. A terrestrial planet's habitability may thus sensitively depend on its short-term climatic stability.

Key words: astrobiology – planetary systems – radiative transfer

Online-only material: color figures

1. INTRODUCTION

The Earth's obliquity is remarkably stable: the angle between the spin axis and the normal to the orbital plane varies by no more than a few degrees from its present value of $\sim 23\overset{\circ}{.}5$. This stability is maintained by torque from the Moon (Laskar et al. 1993; Neron de Surgy & Laskar 1997). Even within our own Solar System, though, the obliquity of other terrestrial planets has varied significantly more; the analysis of Laskar & Robutel (1993) indicates that Mars' obliquity exhibits chaotic variations between $\sim 0^\circ$ and $\sim 60^\circ$.

How does climate depend on obliquity and its possible variations in time? How does the range of orbital radii around a star at which a planet could support water-based life depend on the planet's obliquity? Has the stability of Earth's obliquity made it a more climatically hospitable home? The answers to these questions will be important to evaluate the fraction of stars that have potentially habitable planets. There are now more than 300 extrasolar planets known,[4] several of which are close to the terrestrial regime with masses less than ten times that of the Earth (e.g., Beaulieu et al. 2006; Udry et al. 2007, Bennett et al. 2008; Mayor et al. 2008). *COROT*, which has already launched, and *Kepler*, scheduled to launch in less than 1 year, are dedicated space-based transit-detecting observatories that will monitor a large number of stars to detect the small decreases in stellar flux that occur when terrestrial planets cross in front of their host stars (Baglin 2003; Borucki et al. 2003, 2007). These missions are expected to multiply by perhaps several hundredfold or more the number of known terrestrial planets, depending on the distribution of such planets around Solar-type stars (Borucki et al. 2007, 2003; Basri et al. 2005; although see revised predictions in Beatty & Gaudi 2008). NASA and ESA have plans for ambitious future missions to obtain spectra of nearby Earth-like planets in the hope that they would reveal the first unambiguous signatures of life on a remote world: NASA's *Terrestrial Planet Finder* and ESA's *Darwin* (Leger & Herbst 2007). The design of such observatories, and the urgency with which they will be built and deployed, will depend on the habitability potential of terrestrial planets that will be found in the next 5–10 years.

Over the last 50 years, various authors have addressed how to predict the way in which terrestrial planet habitability depends on star–planet distance (see Kasting & Catling 2003 for a recent review). Several of the important initial calculations predated the first discoveries of extrasolar planets, including Dole (1964), Hart (1979), and the seminal work of Kasting et al. (1993). Selsis et al. (2007), von Bloh et al. (2008), and Barnes et al. (2008) had reconsidered habitability in light of recent exoplanetary detections. Williams et al. (1996), Williams & Kasting (1997, hereafter WK97), and Williams & Pollard (2003) have precisely tackled the questions relating to obliquity posed above, and have concluded that variations in obliquity do not necessarily render a planet uninhabitable (also see Hunt 1982; Williams 1988a, 1988b; Oglesby & Ogg 1998; Chandler & Sohl 2000; Jenkins 2000, 2001, 2003 in the context of Earth's paleoclimate studies).

Here, we seek to generalize these analyses to model planets that are less close analogs to Earth than have been previously considered. In Spiegel et al. (2008, hereafter SMS08), we examined how regionally and temporally habitable climates are affected by variations in the efficiency of latitudinal heat transport on a planet, and by variations in the ocean fraction. Importantly, we found that otherwise habitable Earth-like terrestrial planets

[4] See http://exoplanet.eu/.

can be subject to dynamical climate transitions into globally frozen snowball states. Since it is not trivial to escape a snowball state (e.g., Pierrehumbert 2005) and such globally frozen climates may have profound influences on the development or existence of life (e.g., Hoffman & Schrag 2002), identifying the likelihood of such transitions on terrestrial exoplanets should be central to any habitability assessment. Following in the footsteps of our first analysis, here we focus on obliquity and consider the influence on habitability of several planetary attributes a priori unknown for exoplanets, such as the efficiency of latitudinal heat transport and the land–ocean distribution.

The remainder of this paper is structured as follows. In Section 2, we describe the energy balance climate model we use. In Section 3, we discuss several validation tests in which our model performs well enough to give us some confidence in its behavior for conditions that differ from those found on Earth. In Section 4, we examine the influence on regional and seasonal habitability of various excursions from Earth-like conditions. Finally, we conclude in Section 5.

2. MODEL

In order to describe the surface temperature and its evolution on a terrestrial planet, we use a one-dimensional time-dependent energy balance model based on a diffusion equation for latitudinal heat transport. This type of model has been used in previous investigations of habitable climates (WK97; SMS08), in modeling Martian climate under changes in forcing (Nakamura & Tajika 2002, 2003), and in studies of the Earth's climate (North et al. 1981 and references therein).

Our model is based on the following prognostic equation for the planetary surface temperature (as described in SMS08):

$$C\frac{\partial T[x,t]}{\partial t} - \frac{\partial}{\partial x}\left(D(1-x^2)\frac{\partial T[x,t]}{\partial x}\right) + I = S(1-A). \quad (1)$$

In this equation, $x \equiv \sin\lambda$ is the sine of latitude λ, T is the temperature, C is the effective heat capacity of the surface layer, D is the diffusion coefficient that determines the efficiency of latitudinal redistribution of heat, I is the infrared (IR) emission function (energy sink), S is the diurnally averaged insolation function (energy source), and A is the albedo. Our formalism for insolation on oblique planets follows that of WK97. In the above equation, C, D, I, and A may be functions of T, x, t, and possibly other relevant parameters, respectively.

Our prescriptions for the functions C, D, I, and A follow SMS08 and are largely borrowed from WK97 or the existing geophysical literature on similar energy balance models (EBMs). For simplicity and flexibility, many of our models use very simple, physically motivated prescriptions. As described in SMS08, we find that an IR cooling function of the form

$$I[T] = \sigma T^4/(1 + (3/4)\tau_{\rm IR}[T]) \quad (2)$$

(i.e., a one-zone model combined with a simple Eddington transfer approximation; e.g., Shu 1982) reproduces the greenhouse effect on Earth reasonably well for our purposes. Here, $\tau_{\rm IR}$ represents the opacity of the atmosphere to long wavelength IR radiation. SMS08 described three pairs of IR radiation functions and albedo functions. In this analysis, we will use two of the three: (I_2, A_2), which gives the closest match to the Earth's annual average temperature distribution, and (I_3, A_3), which uses the standard linearized cooling function of North & Coakley (1979). The (I, A) functions are detailed in Table 1.

Table 1
Atmospheric Models

Model	IR Cooling Function	Albedo Function
2[a]	$I_2[T] = \frac{\sigma T^4}{1+(3/4)\tau_{\rm IR}[T]}$	$A_2[T] = 0.525 - 0.245\tanh\left[\frac{(T-268\ {\rm K})}{5\ {\rm K}}\right]$
3[b]	$I_3[T] = A + BT$	$A_3[T] = 0.475 - 0.225\tanh\left[\frac{(T-268\ {\rm K})}{5\ {\rm K}}\right]$
4[c]	$I_{\rm WK97}[T, p{\rm CO_2}]$	$A_2[T]$

Notes. σ is the Stefan–Boltzmann constant.
[a] Model with T-dependent optical thickness: $\tau_{\rm IR}[T] = 0.79(T/273\ {\rm K})^3$.
[b] Linearized model: $A = 2.033 \times 10^5$ erg cm^{-2} s^{-1}, $B = 2.094 \times 10^3$ erg cm^{-2} s^{-1} K^{-1}.
[c] WK97 cooling function (with A_2 albedo). The detailed functional form is presented in the appendix of WK97.

The albedo functions A_2 and A_3 are constant and low ($\sim$0.3) for high temperatures, constant and high ($\sim$0.7) for low temperatures (to represent the high albedo of snow and ice), and vary smoothly in between. Another I function that we use is that proposed in WK97, derived from full radiative–convective calculations, here denoted $I_{\rm WK97}$. This function includes the detailed influence of CO_2 (and implicitly H_2O) atmospheric content on radiative cooling. For C, we assume various configurations of land and ocean; in each configuration, we use the same land, ocean, and ice partial C values as WK97. Finally, we adopt a diffusion coefficient for latitudinal heat transport $D_{\rm fid} = 5.394 \times 10^2$ erg cm^{-2} s^{-1}K^{-1} $\times$ $(\Omega_p/\Omega_\oplus)^{-2}$, as described in SMS08, where Ω_p is the angular spin frequency of the model planet and $\Omega_\oplus$ is that of the Earth. As explained in SMS08, this scaling largely oversimplifies the complexity of atmospheric transport expected for planets at different rotation rates (e.g., del Genio et al. 1993; del Genio & Zhou 1996).

Equation (1) is solved as described in SMS08, on a grid uniformly spaced in latitude (1°25 resolution elements, found to be sufficient from convergence tests). We again choose "hot start" ($T \geqslant 350$ K) initial conditions, to minimize the likelihood that models will undergo a dynamical transition to fully ice-covered (snowball) states from which they cannot recover because of ice-albedo feedback. In that sense, our results on snowball states are conservative.

To summarize, we make the following assumptions in the models presented below.

1. *Heating/Cooling*. The heating and cooling functions are given by the diurnally averaged insolation from a Sun-like ($1\,M_\odot$, $1\,L_\odot$) star, with albedo and insolation functions described above and in Table 1.
2. *Latitudinal Heat Transport*. We test the influence on climate of three different efficiencies of latitudinal heat transport, within the diffusion equation approximation: an Earth-like diffusion coefficient and diffusion coefficients scaled down and up by a factor of 9 (which correspond to 8 hr and 72 hr rotation according to the above $D \propto {\Omega_p}^{-2}$ scaling).
3. *Ocean Coverage*. We vary both the fraction and the distribution of ocean coverage. For ocean fraction, we present a series of models with Earth-like (30%:70%) land:ocean fraction and another series of models that represent a desert world with a 90%:10% land:ocean fraction. For ocean distribution, we present models in which there is a uniform distribution (in every latitude band) of land and ocean, and others in which the land mass is a single continent centered on the North Pole, while the rest of the planet is covered with ocean.

4. *Initial Conditions*. As described in SMS08, all the models have a hot-start initial condition, with a uniform surface temperature of at least 350 K, to minimize the chances of ending up in a globally frozen snowball state owing solely to the choice of initial conditions. Time begins at the northern winter solstice.

3. MODEL VALIDATION

In SMS08, we verified that our "fiducial" model (70% ocean; I_2, A_2 cooling–albedo functions) at 1 AU predicts temperatures that match the Earth's actual temperature distribution at all latitudes that are not significantly affected by Antarctica (i.e., north of 60° S or so). This indicates that the model accounts for the overall (annual) planetary energy balance reasonably well. Another obvious test is whether the model correctly predicts the monthly energy fluxes that together go into the overall balance. Because our current investigation tests the influence of obliquity on climate, and obliquity is the primary driver of the Earth's seasons, verifying the seasonal predictions of our model, given Earth-like conditions, is particularly relevant.

The diffusion equation model is a statement of conservation of energy. By definition, after vertical integration for a thin atmosphere with dominant surface processes,

$$C\frac{\partial T}{\partial t} \equiv \frac{\partial \sigma}{\partial t}, \tag{3}$$

where σ is the energy surface density (internal energy per unit surface area on the globe). The diffusion equation, therefore, says that the rate of change of internal energy at a given point equals the sources of energy (insolation), minus the sinks (IR radiation), minus whatever energy flows away from the point under consideration.

Figure 1 presents a comparison between the annually averaged fluxes of incoming and outgoing radiative energies in the fiducial model with the corresponding fluxes on Earth, taken from NASA's Earth Radiation Budget Experiment (ERBE) in the mid-1980s (Barkstrom et al. 1990).[5] While our model does not capture the full shape of the Earth's cooling and heating functions—in particular, the annually averaged model heating function is a bit below the Earth's at the poles—still, both cooling and heating fluxes are within 10% of the Earth's over most of the planet's surface.

Figure 2 offers an even more compelling validation. In this figure, each of the 12 panels shows solar (i.e., heating), terrestrial (i.e., cooling), and net (solar minus terrestrial) radiative fluxes as functions of latitude, averaged over 1 month. Not only are our annually averaged cooling and heating functions in reasonable agreement with Earth's, as per Figure 1, but furthermore the temporal variability of radiative fluxes in our model is similar to that of Earth.

For example, at the northern winter solstice (upper left panel of Figure 2), the model heating curve closely traces that of the Earth. It peaks at a somewhat more southern latitude than the Earth's, but is within 10% of the Earth's at all latitudes north of 60° S. As the months advance, the concordance between the model heating curve and the Earth's heating curve increases, until there is maximum agreement (within 10% at all altitudes) at the equinox ("Solstice+03"). Then, by the next solstice, the curves agree to within 10% at all latitudes south of roughly 60° N. In a comparison of the cooling curves, the model shows even greater agreement with the data. In a majority of months, these two curves are within 10% of each other at all latitudes.

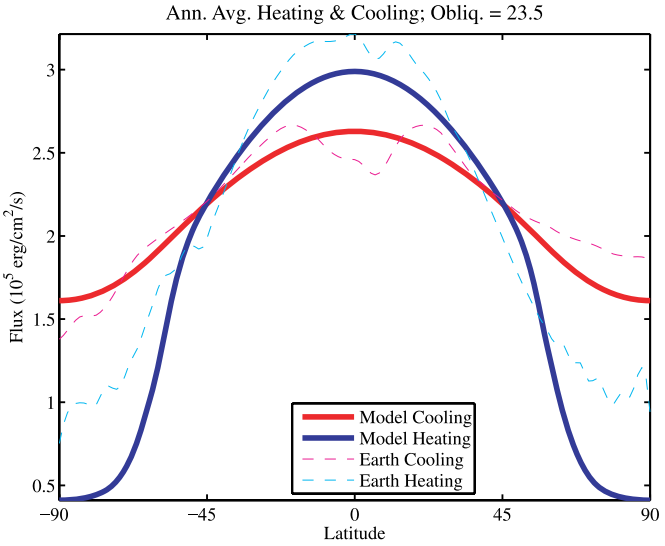

Figure 1. Annually averaged cooling and heating fluxes for our fiducial model at 1 AU and for the Earth. The thick red line is IR cooling and the thick blue line is absorbed solar flux, in our fiducial model (70% uniform ocean, I_2, A_2). The thin dashed magenta line is the Earth's annually averaged long-wavelength IR radiation, and the thin dashed cyan line is the annually averaged absorbed solar flux measured on Earth. Earth-specific features are not captured by our symmetric and uniform model.

(A color version of this figure is available in the online journal.)

Interestingly, the month-by-month variations in model heating and model cooling lead to a net heating curve (heating minus cooling) that predicts some detailed features actually seen in the Earth's net heating budget. Notice, for instance, the slight upward turn of the net heating curves of both the model and the Earth near the North Pole, at and around the northern winter solstice. A similar feature is seen in both curves (though with slightly less impressive detailed agreement) near the South Pole, at and around the southern winter solstice. These comparisons establish that our climate model exhibits reasonable regional and seasonal variability of not just temperature but also incoming and outgoing radiative energy fluxes.

Another way to consider seasonal variations of heating and cooling fluxes is to look at the global average of each with respect to time. Figure 3 presents a comparison of these fluxes, for our fiducial model and the Earth itself. The bottom panel of this figure shows the net heating flux as a function of time of year, measured in fraction of a year from the northern winter solstice. Earth's net heating flux varies by about 5% with respect to the cooling flux, while our model's varies somewhat less. The heating function for the Earth exceeds the cooling function during northern winter for two main reasons as follows.[6] First, the nonzero eccentricity ($e \approx 0.0167$) of the Earth's orbit places its perihelion—which occurs during northern winter—approximately 3.4% closer to the Sun than its aphelion. This is responsible for ∼7% of the ∼10% annual variation in the net heating flux. Our fiducial model, on the other hand, assumes zero eccentricity. Another contributing factor is that the Earth's oceans on average absorb somewhat more insolation than the land, and the Southern Hemisphere—which faces the Sun during

[5] The ERBE satellite measured a short-wavelength, or incoming, flux as that from 0.2 μm to 4.5 μm. A long-wavelength, or outgoing, flux was defined as all other fluxes within the bolometric range of the instrument.

[6] Note that the cooling function, which traces surface temperatures, varies less through the seasonal cycle than the heating function.

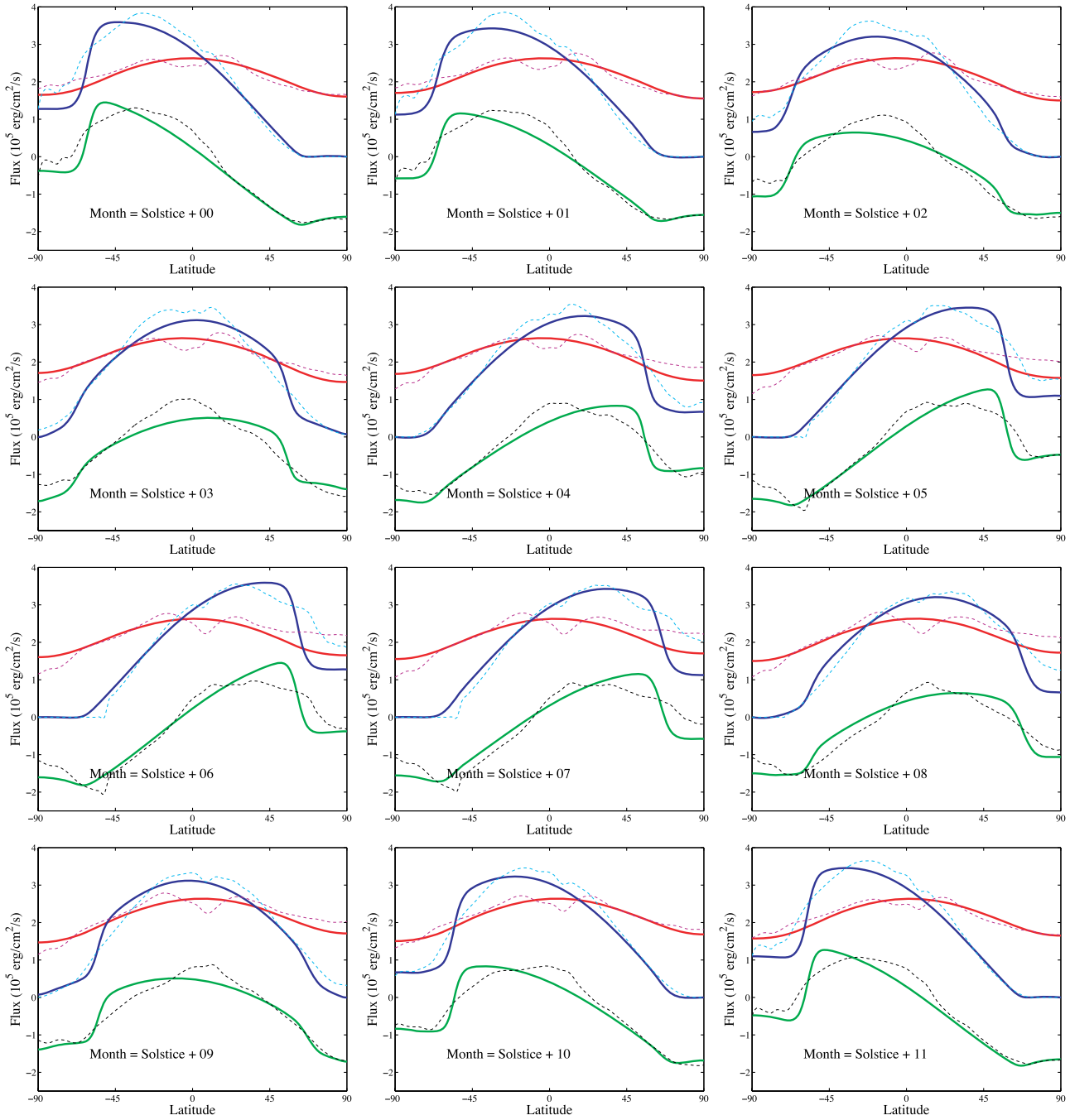

Figure 2. Monthly cooling, heating, and net fluxes for our fiducial model at 23°.5 obliquity and 1 AU orbital distance, and for the Earth. Each panel presents the average cooling, heating, and net (heating minus cooling) radiative fluxes, as functions of latitude, for 1 month of the year, starting at the northern winter solstice (upper left panel), and incrementing by 1 month with each panel to the right. These fluxes are presented for both the model (thick solid lines) and the Earth (thin dashed lines). Model heating is blue, model cooling is red, and model net heating is green. Earth heating is cyan, Earth cooling is deep magenta, and Earth net heating is black. Our model captures reasonably well the seasonal variations of these fluxes.

(A color version of this figure is available in the online journal.)

northern winter—has greater ocean coverage than the Northern Hemisphere. To within 5%, however, the Earth remains in global radiative balance throughout its seasonal cycle.

So far, we have considered the radiative fluxes, but what about diffusive energy flux? We may combine Equation (1) with Equation (3) to produce

$$\frac{\partial \sigma}{\partial t} - \frac{\partial}{\partial x}\left\{D\cos^2\lambda \frac{\partial}{\partial x} T\right\} = (\text{sources} - \text{sinks})_{\text{energy per area}}, \quad (4)$$

where we have substituted $\cos^2\lambda$ for $(1 - x^2)$. Comparing Equation (4) with a diffusion equation in spherical coordinates, and accounting for vertical integration, shows that $F_\lambda = RD\cos\lambda(\partial T/\partial x)$ is the rate of latitudinal energy transport per unit longitudinal length. Therefore, the total rate of meridional diffusive heat transport (i.e., energy crossing a given latitude circle per unit time) is

$$\mathcal{F}_\lambda = 2\pi R\cos\lambda F_\lambda = 2\pi R^2 D\cos^2\lambda \frac{\partial T}{\partial x}. \quad (5)$$

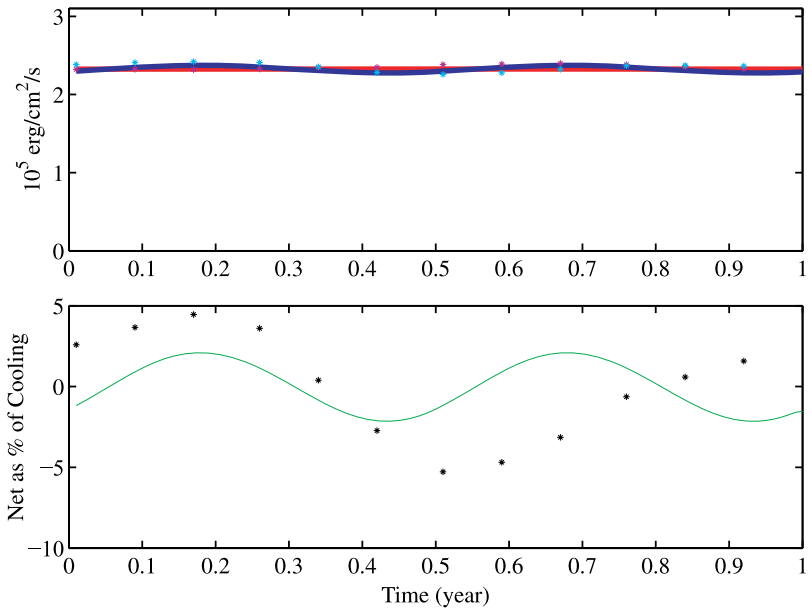

Figure 3. Global average cooling, heating, and net radiative flux as functions of time in our fiducial model at 23°.5 obliquity (solid lines). Earth's ERBE data are shown as stars. Top panel: global average cooling (red curves and magenta stars) and heating (blue curves and cyan stars) fluxes as a function of time of year, measured in fraction of a year from the northern winter solstice. Bottom panel: net heating flux (heating minus cooling) for the model (green curve) and ERBE data (black stars), plotted as percent of the corresponding cooling flux. The Earth remains within 5% of global radiative balance throughout its seasonal cycle.

(A color version of this figure is available in the online journal.)

Figure 4 shows profiles of this diffusive heat transport rate in our fiducial model, at Earth-like 23°.5 obliquity and at extreme 90° obliquity. In the Earth-like configuration, heat flows from the equator toward the poles. In the highly oblique configuration, however, heat flows in the other direction, from the poles to the equator (in an annually averaged sense). For comparison, Williams & Pollard (2003) presented a full general circulation model (GCM) of an Earth-like planet at Earth-like and higher obliquity. Figure 2 of that paper shows the meridional heat flux within their models for 23°.5 and 85° obliquities, and the results are strikingly similar to ours. At 23°.5 obliquity, our model's diffusive flux is very close to that of the GCM. At high obliquity, the flux in our model remains within ∼30% of that in the GCM (from visual inspection), at all latitudes. This reasonable concordance indicates that the treatment of heat transport within our model, despite being very simple, is still likely to remain useful as a representation of heat transport under less Earth-like conditions. We emphasize that it is a nontrivial point that this entirely different regime of transport should remain well captured by a diffusion approximation.

4. STUDY OF HABITABILITY

For model planets with 23°.5 obliquity on a circular orbit at 1 AU, both pairs of IR cooling functions and albedo functions presented in Table 1 are reasonably good matches for the Earth's current climate, as measured by latitudinally averaged temperatures, with a somewhat better fit with (I_2, A_2). This gives us some confidence that these functions are useful guides as to how the climate might respond under different forcing conditions. In this investigation, we consider how variations in intrinsic planetary characteristics combine with the changes in insolation and year length at various orbital radii to map the zone of regionally habitable climates on planets with various obliquities.

We follow SMS08 in saying that, at a given time, a part of a planet is habitable if its surface temperature is between 273 K and 373 K, corresponding to the freezing and boiling points of pure water at 1 atm pressure. This criterion may be criticized for several reasons discussed in SMS08 and references therein, but it provides a reasonable starting point for making numerical investigations. We will frequently quantify the habitability of pseudo-Earths with the temporal habitability fraction, $f_{\rm time}[a, \lambda]$, where a is the orbital semimajor axis, λ is latitude, and $f_{\rm time}$ is the fraction of the year that the point in parameter space specified by (a, λ) spends in the habitable temperature range (see SMS08 for details).

4.1. Efficiency of Heat Transport

Terrestrial planets with different rotation rates will redistribute heat from the substellar point (or, in a one-dimensional model, the substellar latitude) with different efficiencies. According to the idealized scaling described above, wherein the effective diffusion coefficient varies with the inverse square of the planetary rotation rate, slower spinning planets will redistribute heat more efficiently, while faster spinning planets will do so less efficiently. But from where, and to where, is heat redistributed? How does this depend on obliquity and rotation rate? And what influence does this have on climatic habitability?

4.1.1. Direction of Heat Flow

For Earth-like 23°.5 obliquity, the substellar latitude does not vary very much over the course of the year: the tropics are fairly close to the equator (the tropical region is less than one-third of the Earth's surface area). As a result, it is a reasonable approximation that heat is always being transported from the equator to the poles (but see Figure 2 for details). In contrast, on a planet with significantly larger obliquity, the direction of heat flow changes over the course of the annual cycle. At the equinoxes, the equator is the most strongly insolated part of the planet (regardless of obliquity), and so heat builds up at the equator, to be partially redistributed by atmospheric motions. But on a highly oblique planet, polar summers are extremely

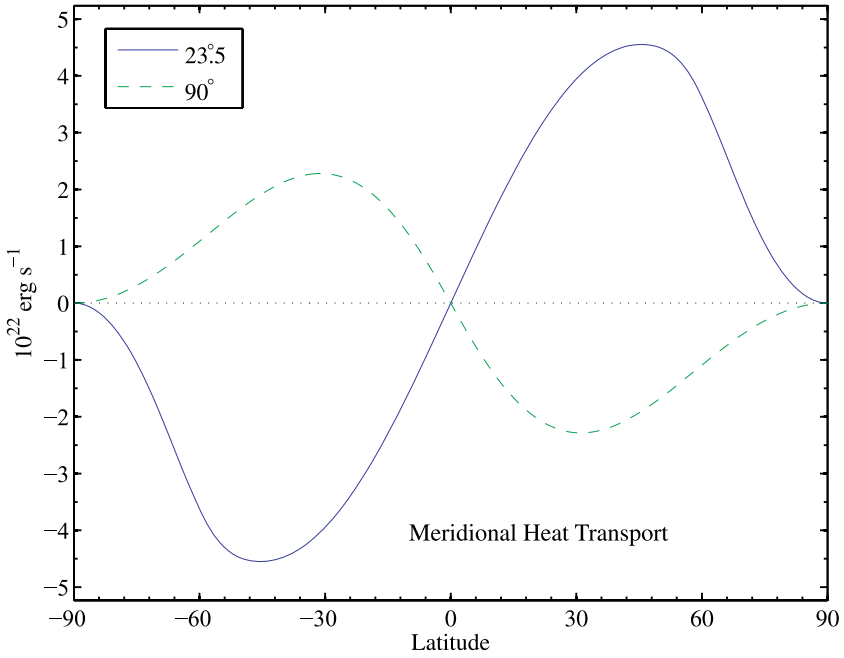

Figure 4. Annually averaged, longitudinally integrated, meridional heat transport rates in models at 23.5 and 90° obliquity. Transport is positive northward. In the Earth-like case (blue solid curve), heat flows from the equator to the poles; in the highly oblique case (green dashed curve), the annually averaged heat flow is reduced and in the opposite direction. This result is in close agreement with a comparable one obtained by Williams & Pollard (2003) with a full-physics climate model.
(A color version of this figure is available in the online journal.)

intense, as measured by diurnally averaged insolation. As a result, heat builds up at the poles during their corresponding summers, and the flow of heat reverses the direction.

Figure 5 demonstrates the effect of such strong polar summers on the global radiation budget of a model planet, by comparison with Figure 1 in which the annually averaged cooling and heating are shown for an Earth-like, 23.5 obliquity model. As expected for the Earth-like model, over the annual cycle, the equator receives significantly more solar radiation than do the poles, and accordingly the annually averaged heating exceeds the cooling at the equator. This indicates that atmospheric motions transport heat poleward from the equator on average. In Figure 5, on the other hand, we present the analogous functions in the case of high and extreme obliquity models. The left panel shows the heating and cooling functions for a model at 60° obliquity; the right panel shows the same functions for a model at 90° obliquity. Planetary scientists have long recognized that in highly oblique models such as these, the polar summers are so intense that, averaged over the year, the most strongly insolated parts of the planet are the North and South Poles! (See, e.g., Ward 1974.) In an annually averaged sense, then, heat flows from the poles to the equator, although clearly the direction of flow changes with the seasons, as described above. The import of these plots is that our notion that the poles are the coldest planetary regions might have to be revised in the case of highly oblique worlds. The resulting regime of atmospheric transport, which is only parameterized with our diffusive treatment, may also be expected to substantially differ from that on Earth (e.g., in terms of equatorial Hadley cells).

Figure 6 shows, in greater detail, the extreme way in which insolation can vary over the annual cycle in a highly oblique model. In this model, the obliquity of an otherwise Earth-like planet (I_2–A_2 functions, with 70% ocean uniformly distributed) is set to 90°. Notice that the cooling remains much more steady than the heating in this model. This is because of the high effective heat capacity of the atmosphere above ocean. In models with less ocean coverage, or oceans that are nonuniformly distributed, the cooling too can dramatically vary over the annual cycle.[7] Because the heating varies so intensely while the cooling varies less, their difference—the net heating curve—also exhibits large variations within the annual cycle. At each solstice, the pole facing the star receives far more net radiant flux than both the opposite pole and the planetary mean. At the equinoxes, something perhaps more surprising happens: the net radiant flux is negative over much of the model planet's surface, and only barely positive near the equator. Overall, the planet heats strongly at the poles during solstices (while cooling elsewhere) and either cools or remains essentially thermally neutral everywhere during equinoxes.

4.1.2. Implications for Habitability

As SMS08 demonstrated, model planets with efficient heat transport (slowly spinning planets) are more latitudinally isothermal than models with Earth-like rotation, which themselves exhibit less latitudinal variation of temperature than those with inefficient heat transport (fast spinning planets). As a result, models corresponding to worlds that are spinning slowly relative to the Earth (but still fast enough so that a one-dimensional climate model has some use) tend to be either entirely habitable or entirely uninhabitable at any given time. In contrast, Earth-like and faster spinning model planets may be only partially habitable at a particular time. They may, for instance, be frozen at the poles and temperate at the equator, or vice versa in the case of a highly oblique world.

Figure 7 demonstrates the complicated interplay that can go on between obliquity and efficiency of heat transport in

[7] It is also worth noting that, at the outer reaches of a $\sim 2\ M_\odot$ star's habitable zone (e.g., Kasting et al. 1993), the annual cycle might be long enough relative to the thermal timescale ($\sim$ a decade) of the ocean–atmosphere mixed layer so that it could undergo relatively large swings in temperature within a single annum.

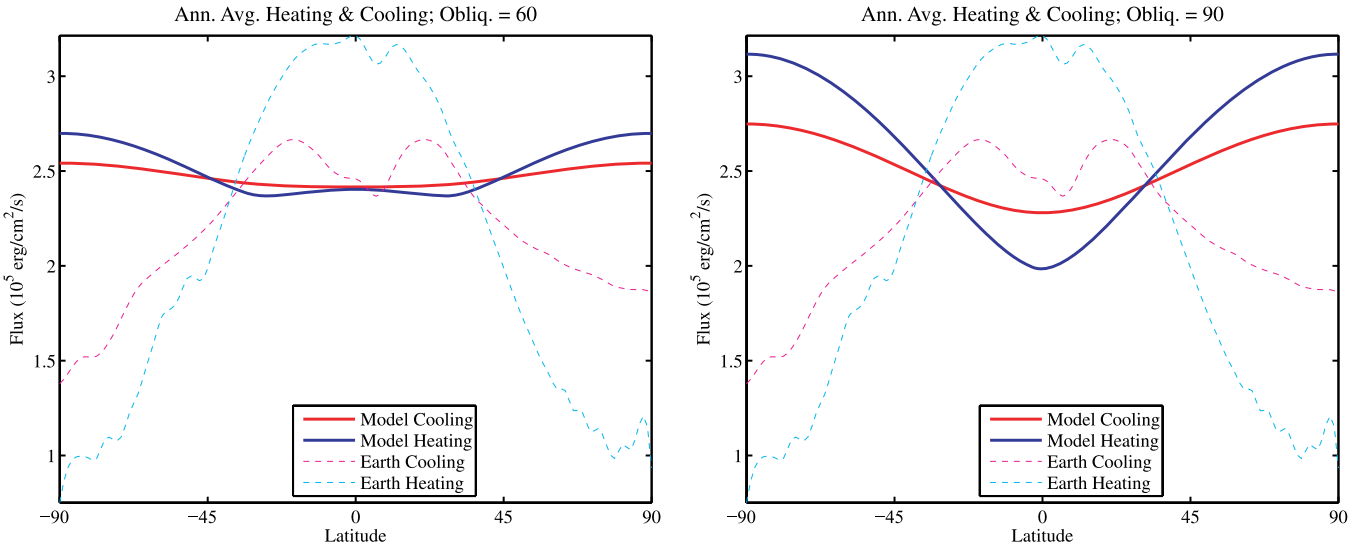

Figure 5. Annually averaged cooling and heating fluxes for high and extreme obliquity model planets, compared to Earth. By contrast with Figure 1, which shows the annually averaged heating and cooling for 23.°5 obliquity, here we present these functions for Earth-like models at 60° obliquity (left panel) and at 90° obliquity (right panel). Thick lines are model results; thin dashed lines are Earth's ERBE data. In both high obliquity cases, unlike on Earth, there is net annually averaged heating at the poles (i.e., heating exceeds cooling) and, especially for the extreme obliquity case, net annually averaged cooling at the equator.

(A color version of this figure is available in the online journal.)

determining a planet's habitability. This figure shows the temporal habitability fraction, as a function of the orbital semimajor axis and latitude, for each of 12 different combinations of obliquity (0°, 30°, 60°, 90°) and latitudinal heat diffusion coefficient ($D_{\rm fid}/9$, $D_{\rm fid}$, and $9D_{\rm fid}$, corresponding, respectively, to 72 hr, 24 hr, 8 hr rotations). The top panel shows these plots for the (I_2, A_2) cooling–albedo pair and the bottom panel depicts the (I_3, A_3) pair (see Table 1 for details). In both panels, the left column of plots represents efficient latitudinal heat transport, the middle column represents Earth-like transport, and the right column represents inefficient transport. Each of the 24 plots in this figure shows the results of model runs for planets located from 0.45 AU to 1.25 AU in increments of 0.025 AU. The color scale indicates the fraction of the year that the latitude at that point spends in the habitable temperature range (273–373 K) on a model planet at the specified orbital semimajor axis. In each plot, the white vertical dashed lines indicate the radiative equilibrium habitable zone, calculated (as discussed in SMS08) from a zero-dimensional model with annually averaged, globally averaged insolation and cooling.

There are a number of interesting features in Figure 7. The most obvious one is that, as expected, at every obliquity, less efficient transport results in more strongly latitudinally differentiated temporal habitability. In addition, at each transport-efficiency value, the $>$ sign shape of the seasonally habitable ribbon at low obliquity reverses to a $<$ sign shape at high obliquity. In other words, at low obliquity, the relatively cold poles are habitable closer to the star and the relatively warm equator is habitable farther from the star. At high obliquity, however, this reverses and the poles are relatively warm, while the equator is comparatively colder.

Furthermore, in both panels, the contours in most cells show a very abrupt outer boundary to the seasonally habitable zone. This is because, as discussed in SMS08, the ice-albedo feedback renders these models quite sensitive to changes in forcing. Small reductions in insolation can be amplified, because the ice coverage increases, which increases the global albedo and leads to further reduction in insolation. This feedback mechanism renders the model climates susceptible to a global snowball transition, from which they cannot recover within our model framework.[8] The main exceptions to this trend are the low obliquity, fast spinning models, in the upper right corners of both panels, although even these models drop to 0% habitability at orbital radii that are small relative to the outer boundary of the habitable zone set by global radiative equilibrium (indicated by the white dashed lines). Interestingly, the fairly small difference in cooling–albedo functions from (I_2, A_2) to (I_3, A_3) is sufficient to allow the cell in the lower right corner of the bottom panel—extreme obliquity, inefficient transport—to avoid transitioning globally to a snowball state. In that model, the intense summer insolation at the poles, combined with the relative thermal isolation of different latitudes, allows the poles to heat up above the freezing point of water during their summers, even at orbital distances where other models would be entirely frozen. In sum, susceptibility to snowball transitions depends on details of parameterizations in our energy balance model, as has been noted before for Earth climate studies (e.g., North et al. 1981).

4.2. Land/Ocean Distribution

As described in SMS08, the large covering fraction of oceans on the Earth (roughly 70%) stabilizes our climate over an annual cycle, by virtue of the large effective heat capacity of atmosphere over ocean. Over land, the thermal relaxation timescale is several months, while for the (∼50 m deep) mixed layer over the ocean, the thermal relaxation timescale is more than a decade. As a result, in a one-dimensional model (such as ours) that does not resolve continents in longitude, any latitude band with significant ocean fraction will have strongly suppressed annual temperature variations relative to a latitude band with low ocean fraction. Because we do not know of any way to determine a

[8] Additional feedback mechanisms that are not incorporated in our model exist on a real planet and might help it to recover from a snowball state. For discussions of how the Earth might have recovered from one or more snowball episodes, see, for example, Caldeira & Kasting (1992), Hoffman & Schrag (2002), and Pierrehumbert (2004).

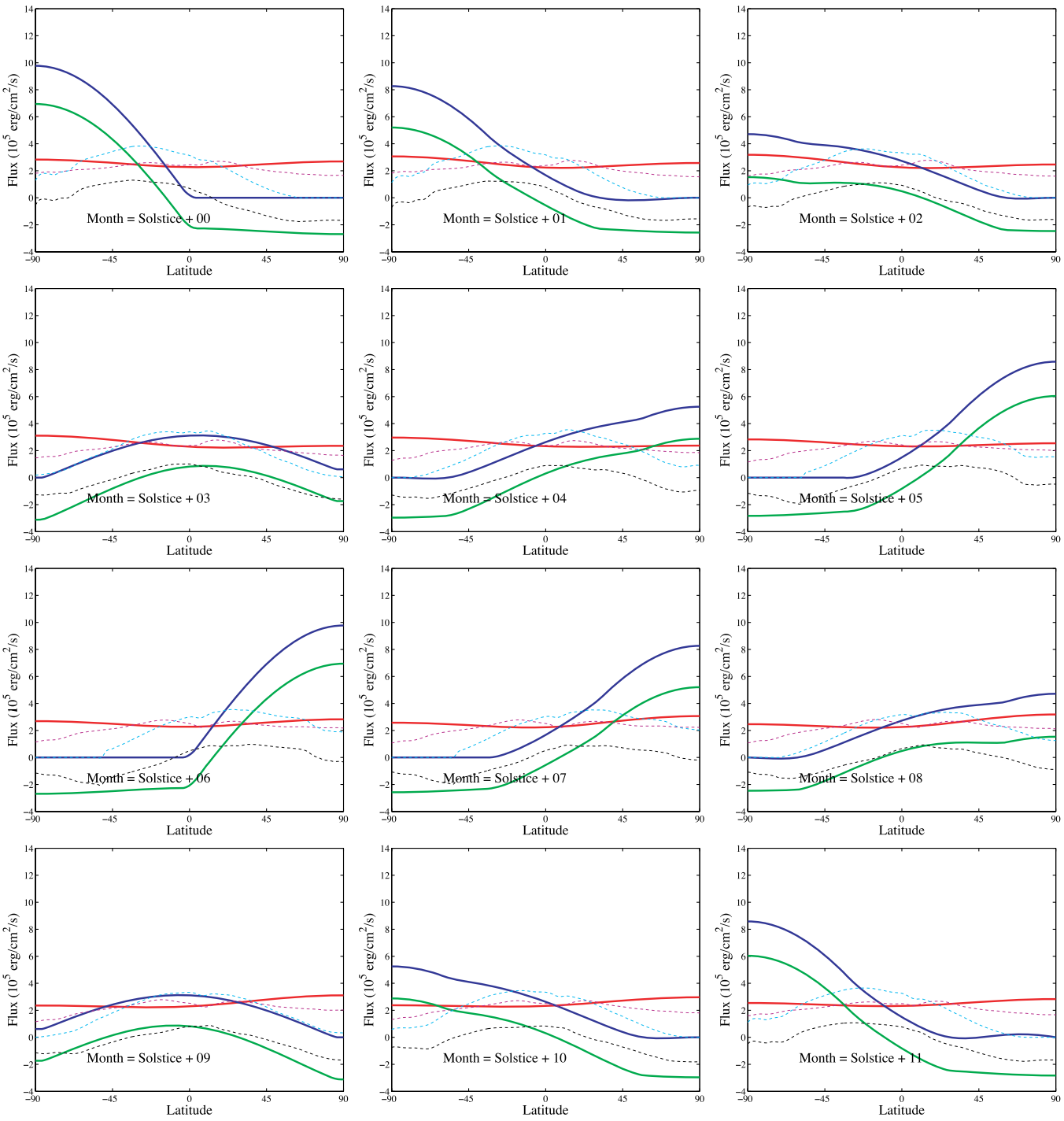

Figure 6. Monthly cooling, heating, and net heating fluxes for the fiducial model at 90° obliquity and 1 AU orbital distance, and for the Earth. Each panel presents the average cooling, heating, and net (heating minus cooling) radiative fluxes, as functions of latitude, for 1 month of the year, starting at the northern winter solstice (upper left panel), and incrementing by 1 month with each panel to the right. These fluxes are shown for both the oblique model planet (thick solid lines) and the Earth (thin dashed lines). Model heating is blue, model cooling is red, and model net heating is green. Earth heating is cyan, Earth cooling is deep magenta, and Earth net heating is black. While cooling fluxes remain relatively steady and uniform on such an oblique planet, heating and net heating fluxes are subject to very large seasonal variations.

(A color version of this figure is available in the online journal.)

priori the distribution of continents and oceans on an extrasolar planet, it is important to consider the influence of other possible land/ocean distributions on climatic habitability.

4.2.1. Nonuniform Ocean Coverage

We consider model planets with distributions of land and ocean that are not uniform across different latitudes: one with 30% land coverage, with a land mass centered on the North Pole (extending down to ∼24° N latitude), and the other (discussed in Section 4.2.2) with 90% land, again centered on the North Pole.[9] Because of the relatively low thermal inertia of atmosphere over

[9] Equivalently, this model can be conceived as having an ocean centered at the South Pole.

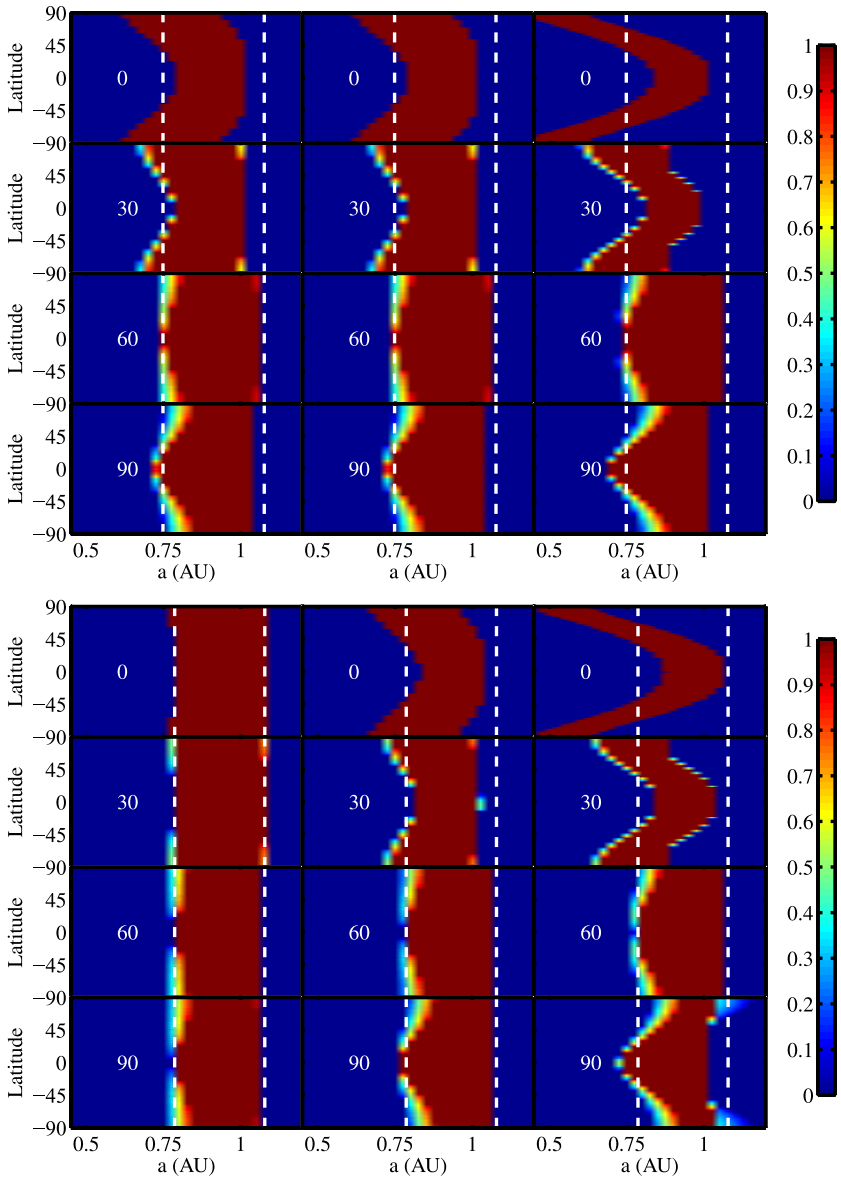

Figure 7. Temporal habitability fraction in models with different obliquities, heat transport efficiencies, and cooling–albedo functions. In both panels, obliquity varies from 0° (top row) to 90° (bottom row). The latitudinal heat diffusion coefficient varies from $9D_{\rm fid}$ (left column) to $D_{\rm fid}$ (center) and $D_{\rm fid}/9$ (right). In each panel, the abscissa is orbital radius, in AU, and the ordinate is latitude. Colors indicate the fraction of the year spent by that region in the habitable temperature range (273–373 K). Top panel: (I_2, A_2) cooling–albedo combination. Bottom panel: (I_3, A_3) cooling–albedo combination. For comparison, vertical dashed lines show the habitable zone extent expected on the basis of global radiative balance. Regionality and seasonality can extend the inner reach of the instantaneous habitable zone while often reducing its outer reach, when global snowball transitions occur.

(A color version of this figure is available in the online journal.)

land, parts of a model planet that are dominated by land can freeze or boil during the course of the year and still return to temperate conditions at other times. In fact, at some orbital distances, and at high obliquity, the polar regions of some models freeze *and* boil within an annual cycle.

Figure 8 displays the tremendous swings of temperature that can occur over latitude bands that lack ocean, and also indicates that annually averaged calculations can miss a lot of information about instantaneous conditions on oblique planets. This figure contrasts the annually averaged temperature with the detailed temperature evolution on a model planet with a North Polar continent that is 30% of the total surface area, at an orbital distance of 1 AU. This model uses (I_2, A_2) cooling–albedo functions, and the results are shown for obliquities 23.5, 60°, and 90°. At all three obliquities, the left column—the annually averaged temperature profile—provides an impoverished view of the actual climatic conditions. Looking at just the left panels, the 23.5 obliquity model appears slightly asymmetrical in temperature distribution, with the continental North Pole 8 K warmer than the oceanic South Pole; the 60° obliquity model appears cooler at the continental pole; and the 90° obliquity model again appears warmer at the continental pole, but appears frozen over the whole globe. In truth, all three models reach significantly higher temperatures at the continental pole during its summer than at the other pole. At both 60° and 90° obliquities, North Pole summer temperatures exceed 410 K, as the Sun shines nearly straight down on the pole for months. We note that an important limitation of our models is apparent in this figure. Although we may not have much intuition for what the polar summers should be like on high obliquity planets,

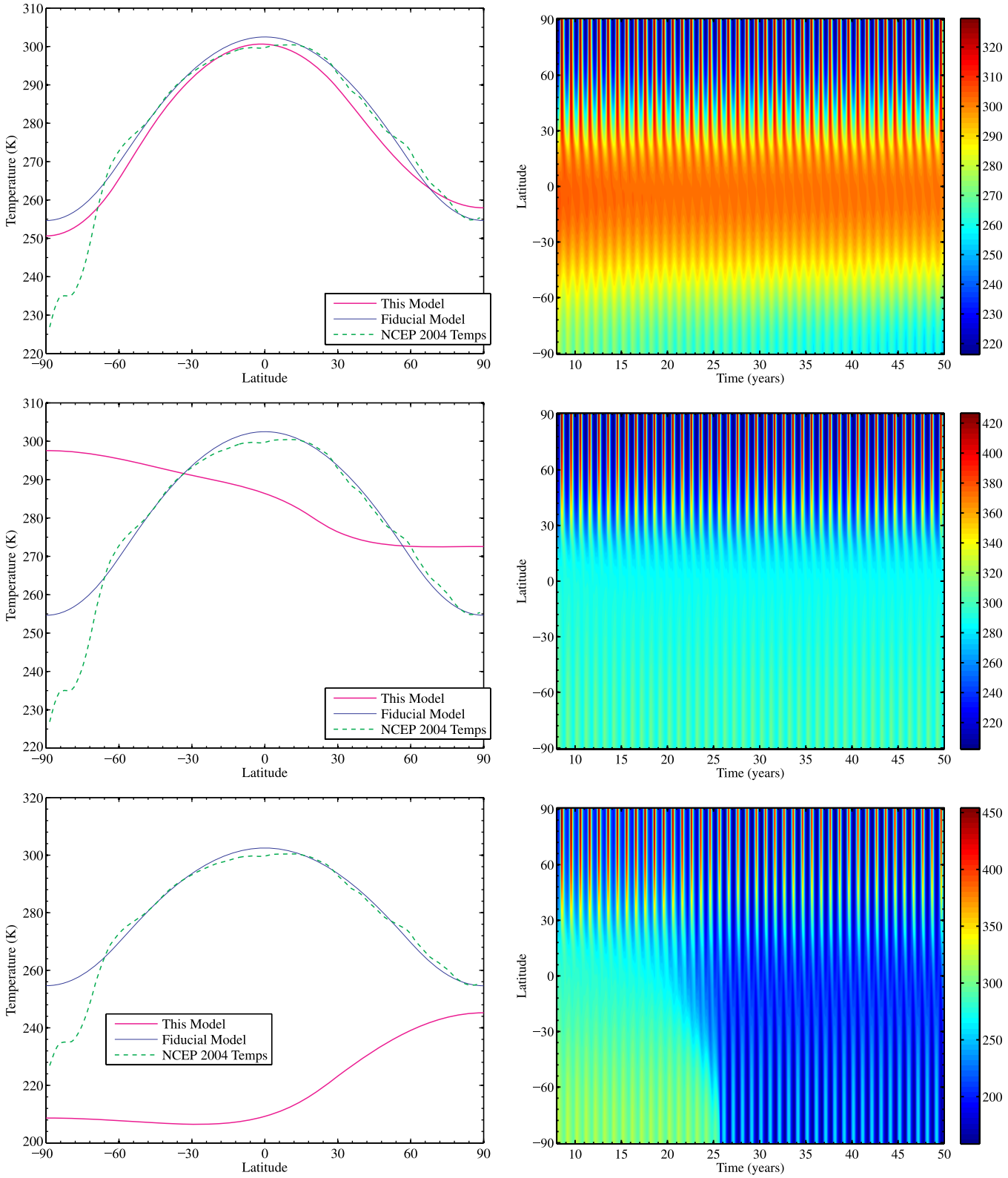

Figure 8. Annually averaged and detailed time-dependent temperature profiles in models with a North Polar continent that takes up 30% of surface area (the other 70% is ocean) at 1 AU orbital distance, for (I_2, A_2) cooling–albedo functions and obliquities of 23.5, 60° and 90°. Left: the magenta curve shows the annually averaged temperature profile for models with a North Polar continent that extends down to ∼24° N latitude. The solid blue and dashed green curves are for reference—blue: the fiducial model (identical to this one, except for 70% ocean uniformly distributed in every latitude band); dashed green: the Earth's actual temperature profile, as measured by NCEP/NCAR in 2004 (Kistler et al. 1999; Kalnay et al. 1996). Right: detailed temperature evolution (latitude vs. time) in the polar continent models from years 8 through 50. Top row: 23.5. Middle row: 60°. Bottom row: 90°. Annually averaged profiles (left) miss much of the seasonal variations shown by the detailed profiles (right). The 90° obliquity model experiences an asymmetric, partial snowball transition.

(A color version of this figure is available in the online journal.)

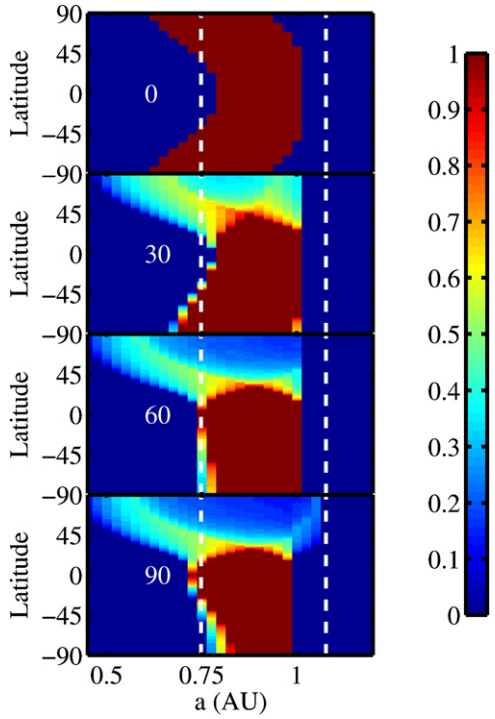

Figure 9. Temporal habitability fraction at different obliquities for a model planet with a North Polar continent covering 30% of its surface. Obliquity varies from 0° to 90° from top to bottom. The latitudinal heat diffusion coefficient is kept to its fiducial value. The notation is similar to Figure 7: colors indicate the fraction of the year spent by that region in the habitable temperature range (273–373 K). Habitability has a strong regional and seasonal character on such a planet, when oblique.

(A color version of this figure is available in the online journal.)

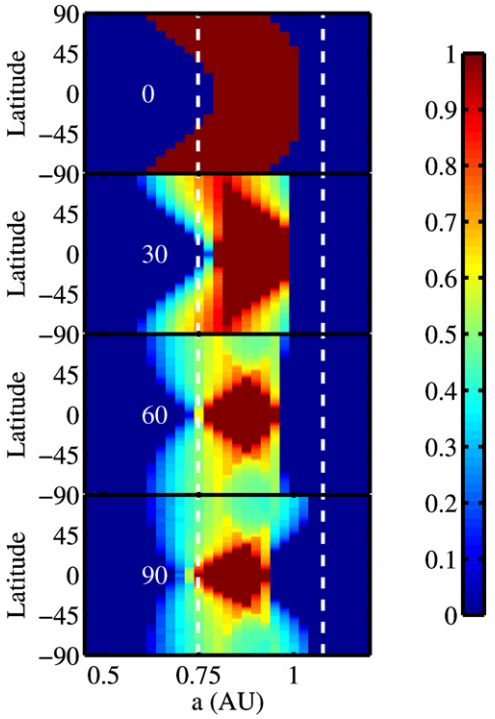

Figure 10. Temporal habitability fraction at different obliquities for a model planet with 10% ocean uniformly distributed. Otherwise, it is similar to Figure 9. Habitability has a strong regional and seasonal character on such a planet, when oblique.

(A color version of this figure is available in the online journal.)

it is surprising to obtain summer polar continent temperatures in excess of 310 K in the 23.5 obliquity model. Indeed, Antarctica—Earth's continental pole—is significantly *colder* than the noncontinental pole, and for the most part, neither pole ever reaches temperatures above freezing. Accounting for Antarctica in our model framework would be nontrivial, as it might require initial conditions differing from uniformly ice-free and/or improved treatments of ice-related surface processes.

Figure 9 presents plots of the temporal habitability fraction for the same model planet as above, at obliquities 0°, 30°, 60°, and 90°. Figure 8 illustrates how the presence of land at the North Pole causes tremendous swings in temperature there; Figure 9 confirms that, for nonzero obliquity, this is indeed the case throughout the orbital extent of the habitable zone. These large seasonal variations lead to exotic shapes in plots of temporal habitability. Compared with uniformly ocean-dominated worlds, much more of the parameter space is partially habitable at each obliquity (except 0°), neither 0% nor 100% of the year, but somewhere in between.

4.2.2. Desert Worlds

We now consider two model planets with just 10% ocean fraction. We examine the cases of a uniformly distributed ocean (10% in every latitude band) and an ocean localized at the South Pole (extending northward to ∼53° S latitude). Figure 10 presents the temporal habitability for the uniform desert world, while Figure 11 presents the analogous plot for the desert world with a South Polar ocean. As before, some regions of these model planets swing from freezing to boiling temperatures over the course of the year. This is responsible for the butterfly shape of the temporal habitability plots in the 60° and 90° obliquity cases shown in Figure 10: at $a \sim 0.9$ AU, the poles are habitable for a smaller fraction of the year than more equatorial regions at that orbital distance, or than the poles for closer and more distant orbits. The pattern of habitability in Figure 11, on the other hand, shows how strongly asymmetric the climate can be on a desert world with a polar ocean.

These models, and those presented in Section 4.2.1, suggest that at extreme obliquity the inner edge of the zone of regionally and seasonally habitable climates can be extended dramatically inward, while the outer boundary can only be extended mildly outward. Several important caveats should accompany this observation, however. Assuming an IR cooling function that is constant with orbital radius probably leads to a flawed treatment at both the high and the low insolation limits of these models. At the inner edge of the habitable zone, large increases in the atmospheric water content can cause a reduction in the cooling efficiency, leading to a runaway greenhouse effect. An eventual catastrophic water loss can result in a Venus-like outcome, as described by Kasting et al. (1993) and references therein (although this type of outcome might be mitigated by reduced heating from increased cloud-albedo, as mentioned in SMS08). At the outer edge, on long timescales, a reduced efficiency of the carbonate–silicate weathering cycle is likely to lead to a significant increase in the partial pressure of atmospheric CO_2 (Kasting et al. 1993), which could extend the habitable zone from ∼1 AU, as in our models, to ∼1.4 AU or beyond in some cases. In Section 4.3, we discuss, in greater detail, the issue of varying atmospheric CO_2 content with orbital distance.

Notwithstanding these various complications, for plausible cooling functions, the low thermal inertia of atmosphere over

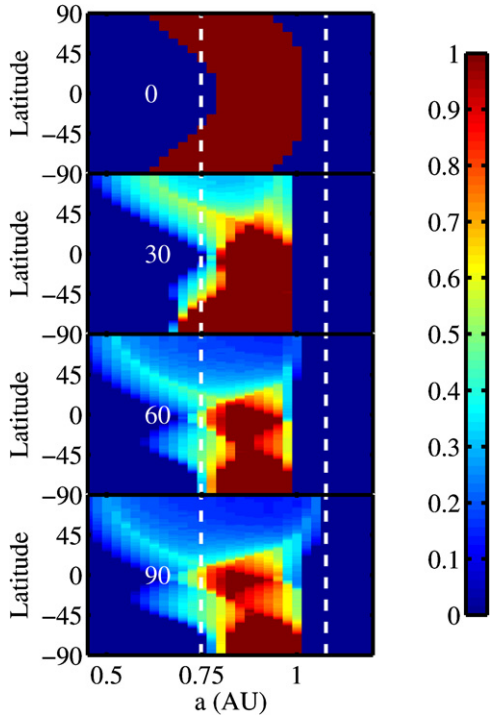

Figure 11. Temporal habitability fraction at different obliquities for a model planet with a North Polar continent covering 90% of its surface (i.e., a localized South Polar ocean). Otherwise, it is similar to Figure 9. Habitability has a strong regional and seasonal character on such a planet, when oblique.

(A color version of this figure is available in the online journal.)

land might lead to severe polar climates on highly oblique planets. What are we to make of partial "habitability" by our criterion in the case of a region of a planet that actually boils and freezes every year? There are some microbes on Earth that can reproduce at freezing temperatures and some that can reproduce at boiling temperatures (see SMS08 and references therein), although none of which we are aware that can do both. If part of a planet regularly swings through these wild extremes of climate, is it appropriate to call it habitable? More relevant from the perspective of formulating a testable scientific hypothesis, could such a planet support enough life to produce sufficient levels of biosignatures that its life could be detected from Earth? This is an open question, but it is worthwhile to keep in mind that microbes on Earth appear to be as hardy as they need to be: nearly everywhere that biologists have searched, they have found some microbes thriving. A perhaps equally significant result from the perspective of habitability is that the reduced thermal inertia of these models appears to render them somewhat less susceptible to global snowball events, especially at high obliquities (e.g., compare Figures 9–11 with the middle column of Figure 7).

4.3. Modeling the Far Reaches of the Habitable Zone

Walker et al. (1981) proposed that a planet's temperature is regulated on long timescales by a feedback mechanism involving weathering of silicate rocks through carbonic acid from CO_2 dissolved in water. They argued that, since the rate of weathering (and hence of removal of CO_2 from the atmosphere) increased with temperature, this process is an important negative feedback on climate that acts to keep temperatures near the freezing point of water (see the recent study by Zeebe & Caldeira (2008) confirming the operation of this cycle). Kasting et al. (1993) pointed out that this negative feedback can significantly offset the extreme sensitivity of climate to changes in orbital distance away from 1 AU seen in models such as those of Hart (1979) and the models presented in SMS08 and thus far in this paper. These models are sensitive because they contain a significant positive feedback of the Earth's climate—the ice-albedo feedback whereby at lower temperatures, the absorbed insolation is dramatically reduced because of the high albedo of ice. However, these models also ignore the long-term, negative (counterbalancing) feedback of the carbonate–silicate weathering cycle (Kasting et al. 1993).

In order to probe the combined influence on the climate of rotation rate and obliquity in the context of the expected CO_2-rich atmosphere that a pseudo-Earth would have at 1.4 AU, we switch to the IR cooling function used by WK97 (I_{WK97} in Table 1), with CO_2 partial pressure (pCO_2) set to 1 bar and 2 bars. For simplicity, we maintain the same albedo function A_2 as before and adopt the same linear dependence of the latitudinal heat diffusion coefficient with the total atmospheric pressure as WK97 ($D/D_{fid} \propto P_{tot}$). We find that at both 1 and 2 bar levels of CO_2, model planets maintain globally temperate conditions at all obliquities for both $D = 9D_{fid}$ and $D = D_{fid}$, corresponding to slow and Earth-like rotation, respectively. Interestingly, however, at reduced transport efficiency, corresponding to fast planetary rotation, we find that these CO_2-rich models are susceptible to global glaciation events.

Figure 12 shows the global average temperature and the climate evolution for fast spinning model planets at 1.4 AU with 1 bar atmospheric CO_2 (I_{WK97}, A_2), cooling–albedo functions, and a latitudinal heat diffusion coefficient scaled up with total pressure but reduced by a factor of 9 to account for rapid rotation. At 23.°5 obliquity, the cold temperatures at the poles drag the model to a snowball state, while at 90° obliquity, it is the cold equator that drags the model planet to the same fate. At 60° obliquity, however, no part of the planet receives consistently low enough insolation to trigger global glaciation. The snowball effect seen in the 23.°5 and 90° obliquity models might be particularly dramatic because of the possibility of partial atmospheric collapse, on a much shorter timescale than volcanism can replenish CO_2. At 1 bar, the freezing point of CO_2 is ∼195 K. Both the 23.°5 and 90° obliquity models reach temperatures below this threshold over large enough regions of their surfaces[10] that significant amounts of the atmospheric CO_2 might condense out as dry ice, thereby reducing the atmospheric greenhouse effect. The risk of atmospheric collapse would be somewhat lessened by the release of latent heat from CO_2 condensation, which would tend to prevent too much CO_2 from freezing out during any winter. Partial collapse, on the other hand, would reduce surface pressure and thus the efficiency of atmospheric heat transport. Realistically treating these possibilities is beyond the scope of the present paper as it would require incorporating a latent heat term in the energy balance equation and accounting for the surface CO_2 mass budget, as Nakamura & Tajika (2002) did in their Mars EBM.

While model runs with 2 bars of CO_2 (not shown) indicate that a pseudo-Earth with such a massive atmosphere at 1.4 AU would be unlikely to suffer glaciation or partial atmospheric collapse at any obliquity, it is worth noting that on a planet with a rate of volcanic greenhouse gas output not much higher than on Earth, it might be difficult to build up a thick CO_2 atmosphere

[10] The very large seasonal variations of temperature on these snowball planets result from the moderate heat capacity of the atmosphere over ice (see, e.g., SMS08; WK97).

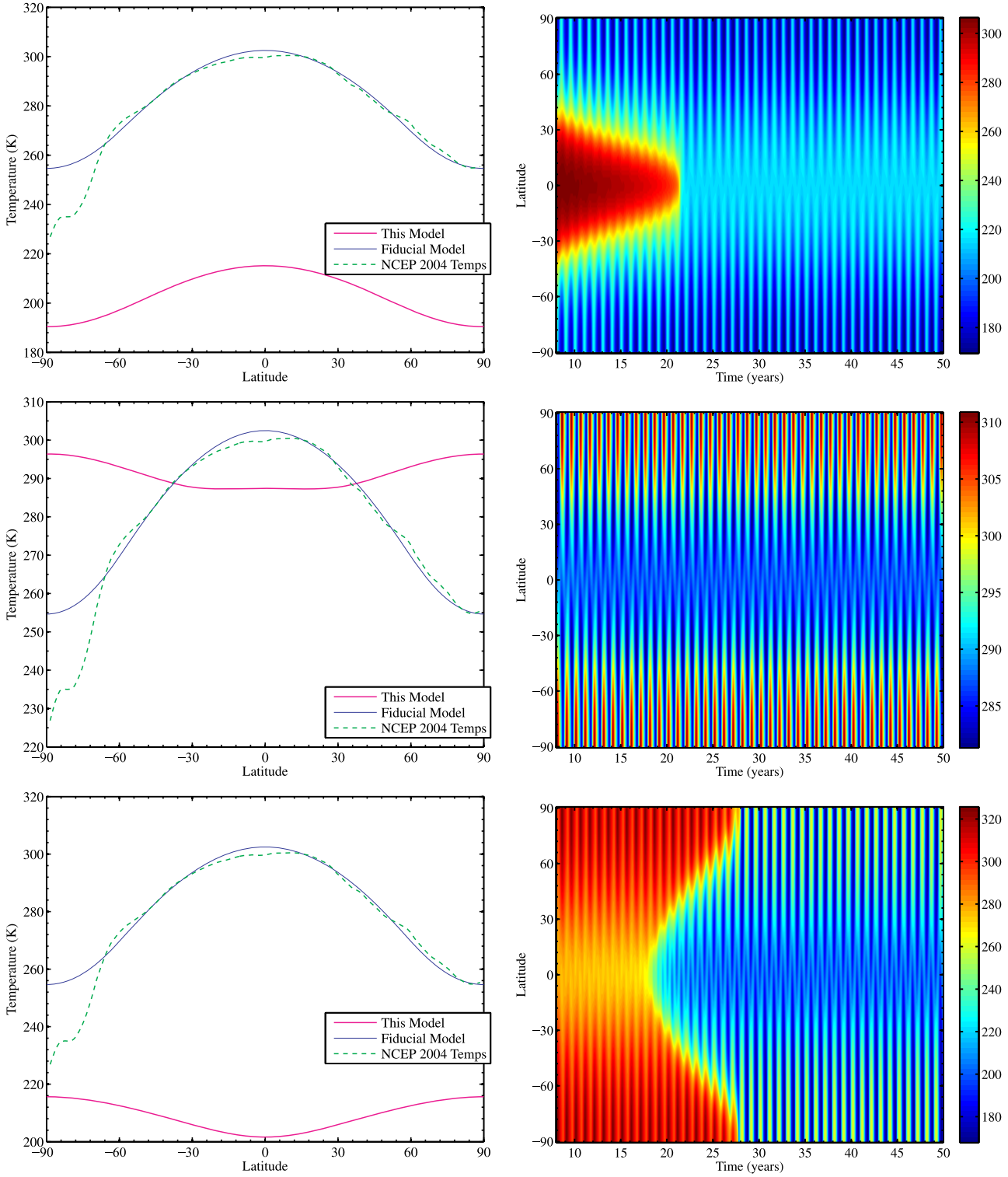

Figure 12. Annually averaged and detailed time-dependent temperatures on a fast spinning model planet at 1.4 AU, using the IR cooling function of WK97 for a CO_2-rich atmosphere with $pCO_2 = 1$ bar. From top to bottom, results are shown for an obliquity of 23.5, 60°, and 90°. The notation and the models are the same as in Figure 8, except for the cooling function (I_{WK97} with $pCO_2 = 1$ bar) and a latitudinal heat diffusion coefficient adjusted for fast spin and a massive atmosphere. In the two globally frozen models (top and bottom), surface temperatures that would result in seasonal CO_2 atmospheric collapse ($T \lesssim 195$ K) are reached over a fair fraction of the planet's surface area.

(A color version of this figure is available in the online journal.)

(e.g., 2 bars) under conditions such that CO_2 condenses out at lower pressure (like in our model with 1 bar of CO_2). In situations in which atmospheric CO_2 concentrations can appreciably change on a yearly timescale, our model is not self-consistent. Further analysis is therefore needed to determine the full extent and consequences of such atmospheric condensation events. Clearly, these various issues are important subjects for future studies since they indicate that snowball transitions could,

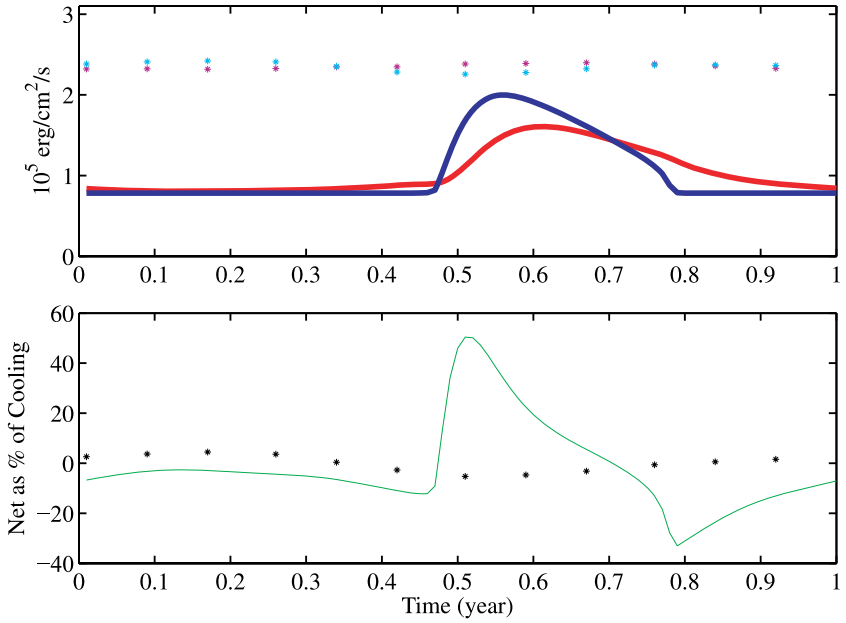

Figure 13. Global average cooling, heating, and net (heating minus cooling) radiative flux, as functions of time, for a model planet with a North Polar continent covering 30% of its surface, at 90° obliquity. Notation is similar to Figure 3. This planet experiences large deviations from global radiative balance.
(A color version of this figure is available in the online journal.)

in principle, limit the habitability of some terrestrial planets by interfering with the negative feedback of their carbonate–silicate weathering cycles.

4.4. Validity of Global Radiative Balance

Calculations of habitable zones have often assumed global radiative balance conditions. Although these calculations by definition cannot account for the regional character of habitability, one might hope that they still provide a decent proxy for the global average conditions. Indeed, as seen in Figure 3, the Earth itself is within ∼5% of radiative equilibrium throughout the year. Accordingly, global radiative balance models have provided a very useful starting point for considerations of how the habitability of an Earth-like planet depends on its orbital radius.

Figure 13 presents globally averaged cooling, heating, and net radiative fluxes in a model with a North Polar continent that covers 30% of the planet's surface, with 90° obliquity. In contrast to the Earth, which remains within 5% of global radiative balance, this model planet can be nearly 60% out of global radiative balance. While it has been recognized that planets on highly eccentric orbits experience forcings that are significantly different from annually and globally averaged conditions, the results in Figure 13 illustrate how, even on circular orbits, planets can experience conditions that are far from radiative equilibrium. This further underscores the importance of regional, time-dependent climate models for addressing the habitability of extrasolar terrestrial planets.

5. CONCLUSIONS

We have presented a series of energy balance models to address the variety of climatic conditions that might exist on oblique terrestrial planets with circular orbits. We considered dynamic climate forcings and responses determined by several planetary attributes a priori unknown for extrasolar planets, including obliquity, rotation rate, distribution of land/ocean coverage, and the detailed nature of the radiative cooling and heating functions. We find that planets with small ocean fractions or polar continents can experience very severe seasonal climatic variations, but that these planets also might maintain seasonally and regionally habitable conditions over a larger range of orbital radii than more Earth-like planets. Climates on high obliquity planets with nonuniform distributions of land and ocean can be far from global radiative balance, as compared to the Earth. Our results provide indications that the modeled climates are somewhat less prone to dynamical snowball transitions at high obliquity. Fast rotating Earth-like planets may fall victim to global glaciation events at closer orbital radii than slower rotating planets. This is also the case for planets with massive CO_2 atmospheres, which are expected to be found in the outer orbital range of habitable zones. Snowball transitions could be particularly significant for such planets since partial collapse of their CO_2-rich atmospheres may occur and possibly interfere with the thermostatic effect of their carbonate–silicate weathering cycle, thus affecting their long-term habitability.

We acknowledge helpful conversations with James Cho, Michael Allison, Anthony Del Genio, and Scott Gaudi. We thank Diana Spiegel for help with ERBE data. D.S. acknowledges support in part from NASA grant NNX07AG80G. C.S. acknowledges the funding support of the Columbia Astrobiology Center through Columbia University's Initiatives in Science and Engineering, and a NASA Astrobiology: Exobiology and Evolutionary Biology; and Planetary Protection Research grant, # NNG05GO79G.

REFERENCES

Baglin, A. 2003, Adv. Space Research, 31, 345
Barkstrom, B. R., Harrison, E. F., & Lee, R. B., III. 1990, EOS Trans., 71, 279
Barnes, R., Raymond, S. N., Jackson, B., & Greenberg, R. 2008, Astrobiol., 8, 557
Basri, G., Borucki, W. J., & Koch, D. 2005, New Astron. Rev., 49, 478
Beatty, T. G., & Gaudi, B. S. 2008, ApJ, 686, 1302

Beaulieu, J.-P., et al. 2006, Nature, 439, 437
Bennett, D. P., et al. 2008, ApJ, 684, 663
Borucki, W. J., et al. 2003, in ESA Special Publication 539, Earths: DARWIN/TPF and the Search for Extrasolar Terrestrial Planets, ed. M. Fridlund, T. Henning, & H. Lacoste, 69
Borucki, W. J., et al. 2007, in ASP Conf. Ser. 366, Transiting Extrapolar Planets Workshop, ed. C. Afonso, D. Weldrake, & T. Henning (San Francisco, CA: ASP), 309
Caldeira, K., & Kasting, J. F. 1992, Nature, 359, 226
Chandler, M. A., & Sohl, L. E. 2000, J. Geophys. Res., 105, 20737
del Genio, A. D., & Zhou, W. 1996, Icarus, 120, 332
del Genio, A. D., Zhou, W., & Eichler, T. P. 1993, Icarus, 101, 1
Dole, S. H. 1964, in Habitable Planets for Man (New York: Blaisdell Pub. Co.)
Hart, M. H. 1979, Icarus, 37, 351
Hoffman, P. F., & Schrag, D. P. 2002, Terra Nova, 114, 129
Hunt, B. G. 1982, J. Meteor. Soc. Japan, 60, 309
Jenkins, G. S. 2000, J. Geophys. Res., 105, 7357
Jenkins, G. S. 2001, J. Geophys. Res., 106, 32903
Jenkins, G. S. 2003, J. Geophys. Res. (Atmospheres), 108, 4118
Kalnay, E., et al. 1996, Bull. Am. Meteor. Soc., 77, 437
Kasting, J. F., & Catling, D. 2003, ARA&A, 41, 429
Kasting, J. F., Whitmire, D. P., & Reynolds, R. T. 1993, Icarus, 101, 108
Kistler, R., et al. 1999, Bull. Am. Meteor. Soc., 82, 247
Laskar, J., Joutel, F., & Robutel, P. 1993, Nature, 361, 615
Laskar, J., & Robutel, P. 1993, Nature, 361, 608
Leger, A., & Herbst, T. 2007, arXiv:0707.3385
Mayor, M., et al. 2008, arXiv:0806.4587
Nakamura, T., & Tajika, E. 2002, J. Geophys. Res. (Planets), 107, 5094
Nakamura, T., & Tajika, E. 2003, Geophys. Res. Lett., 30, 18
Neron de Surgy, O., & Laskar, J. 1997, A&A, 318, 975
North, G. R., Cahalan, R. F., & Coakley, J. A., Jr. 1981, Rev. Geophys. Space Phys., 19, 91
North, G. R., & Coakley, J. A. 1979, Evolution of Planetary Atmospheres and Climatology of the Earth, 249
Oglesby, R. J., & Ogg, J. G. 1998, Paleoclimates, 2, 293
Pierrehumbert, R. T. 2004, Nature, 429, 646
Pierrehumbert, R. T. 2005, J. Geophys. Res. (Atmospheres), 110, 1111
Selsis, F., Kasting, J. F., Levrard, B., Paillet, J., Ribas, I., & Delfosse, X. 2007, A&A, 476, 1373
Shu, F. H. 1982, The Physical Universe. An Introduction to Astronomy (A Series of Books in Astronomy) (Mill Valley, CA: University Science Books)
Spiegel, D. S., Menou, K., & Scharf, C. A. 2008, ApJ, 681, 1609
Udry, S., et al. 2007, A&A, 469, L43
von Bloh, W., Bounama, C., Cuntz, M., & Franck, S. 2008, in IAU Symp. 249 (Dordrecht: Kluwer), 503
Walker, J. C. G., Hays, P. B., & Kasting, J. F. 1981, J. Geophys. Res., 86, 9776
Ward, W. R. 1974, J. Geophys. Res., 79, 3375
Williams, D. M., & Kasting, J. F. 1997, Icarus, 129, 254
Williams, D. M., Kasting, J. F., & Caldeira, K. 1996, in Circumstellar Habitable Zones, ed. L. R. Doyle, 43
Williams, D. M., & Pollard, D. 2003, Int. J. Astrobiol., 2, 1
Williams, G. P. 1988a, Climate Dyn., 2, 205
Williams, G. P. 1988b, Climate Dyn., 3, 45
Zeebe, R.-E., & Caldeira, K. 2008, Nature Geosci., 185, 312